The International Journal of Advanced Manufacturing Technology (2022) 120:8169–8184
https://doi.org/10.1007/s00170-022-09019-0

ORIGINAL ARTICLE

Dross formation modeling in the laser beam cutting process using energy-based and gas-based parameters

Seyedeh Fatemeh Nabavi[1] · Mohammad Hossein Farshidianfar[1] · Anooshiravan Farshidianfar[1] · Saeed Marandi[1]

Received: 28 May 2021 / Accepted: 6 March 2022 / Published online: 7 May 2022

Abstract

Dross formation in the laser beam cutting (LBC) process is modeled in the present study using two main categories of parameters: (1) energy-based (e.g., laser power, scanning velocity, and focal position) and (2) gas-based (e.g., assisting gas pressure, the diameter of the nozzle, and workpiece distance). A set of comprehensive analytical and empirical models is developed to predict dross diameter during the LBC process based on these groups of parameters. First, a novel closed-form analytical model of the dross diameter based on the energy balance approach is presented. The model considers heat loss during the cutting process in terms of conduction, radiation, and evaporation latent heat energy that has not been addressed in the literature. Furthermore, regression and physical parameter modeling methods are used to develop two empirical models. The regression model includes all effective gas-based and energy-based processing parameters. In the physical model, two unique physical parameters are introduced that provide physical insight into the process. The amount of energy radiated per unit area and the amount of gas deposited per unit area is represented by energy density and gas density parameters, respectively. All models are validated by laser fiber cutting experiments on austenitic stainless steel. The accuracy of the analytical model is compared with a previous study, which indicates a reduced error as a result of considering all main heat loss terms. The results reveal that the dross diameter is dominated by gas-based rather than energy-based processing parameters.

Keywords Laser beam cutting · Regression model · Analytical model · Combined physical parameter model · Energy-based parameters · Gas-based parameters · Austenitic stainless steel

Nomenclatures

Parameter	Definition
ε	Emissivity of the surface of the material
σ	Stefan-Boltzman constant
β	Fraction of evaporation contribution
ρ_{G}	Density of assisting gas
μ_{G}	Viscosity of assisting gas
μ_{L}	Viscosity of melting material
ρ_{L}	Density of melted workpiece
A	Cross-section area
C_{pm}	Specific heat capacity of the material in the liquid state
C_{ps}	Specific heat capacity of the material in the solid-state
d	Workpiece distance
d_{D}	Dross diameter
ED	Energy density of laser cutting process
F	Focal position
g	Assisting gas pressure
GD	Gas density of laser cutting process
K	Material conductivity
L_{ev}	Latent heat of boiling
L_{m}	Latent heat of melting
N	Diameter of nozzle
P	Laser power
S_{L}	Liquid thickness layer
T_{i}	Initial temperature
T_{m}	The melting temperature
T_{ev}	Vaporization temperature of the material
v	Laser scanning velocity

✉ Anooshiravan Farshidianfar
farshid@um.ac.ir

Seyedeh Fatemeh Nabavi
s.fa.nabavi@alumni.um.ac.ir

Mohammad Hossein Farshidianfar
farshidianfar@um.ac.ir

Saeed Marandi
saeid.marandi.74@gmail.com

[1] Mechanical Engineering, Ferdowsi University of Mashhad, Mashhad, Iran

$\mathbf{v_G}$	Velocity of the gas jet
z	Material thickness

1 Introduction

Laser beam cutting (LBC) is a thermal process that involves applying the laser beam to cut the material. LBC process can be classified into heating, melting-vaporizing, and ejection stages. In the first stage, the focused laser beam heats the surface of the workpiece. The power of the laser beam is enough to start melting, forming the molten layer, and vaporizing process (second stage). Then high-pressure assisting gas is used to blow the molten metal out of the kerf in the last stage [1]. These stages in the LBC process provide a variety of advantages, namely low power consumption, high machining speed, no need to clamp parts, no tool wear, no vibration, and not having any limitation in material workpiece [2–5]. Hence, the LBC process becomes a routine process in fabrication [6]. Since laser cutting technology is novel, in-depth study of all its significant challenges has yet to be addressed in the literature. One of the biggest challenges of the LBC process is a dross formation, which may cause different problems in plate heat exchangers and the aerospace industry. However, minimal research has been conducted on the dross of the LBC process and its overall characteristics.

Since all laser material processing technologies, including LBC, have specific input parameters, the initial step towards achieving a fully controlled model of the dross is to understand the effective input processing parameters. The processing parameters, which affect dross, can be divided into energy-based and gas-based parameters. The energy-based parameters provide the needed energy of heating and melting stages (first and second stages), while the ejection of melt materials is obtained by gas-based parameters (third stage) [1].

Dross is an undesirable projection of material on the edge of the cut, which is produced because of plastic flow in the laser beam cutting process [7–9]. The dross has various effects on systems, including the component fitting issues in assembly, fouling inflow of systems, employee's injuries, and inappropriate appearance [7, 10]. All of these reduce efficiencies of the LBC process. Thus, a tailor-made model, which predicts the dross formation during the process, is needed.

Melt formation and dross diameter during LBC of the metallic workpiece are formulated analytically by Yilbas and Abdul Aleem [11]. Melt energy, including laser beam, oxidation, conduction, and requirement energies (energy needs to melt and evaporation materials), was considered in their model. Energy balance in their model leads to the dross diameter formula by measuring edge boundary layer velocity. Schuöcker et al. [12] propose a shear stress formula, which was used in the dross diameter model of a study presented by Teixidor et al. [6]. Their analytical dross diameter model was based on energy balance, including laser beam and convection. Since increasing laser power leads to increased portion of evaporation, radiation, and conduction energies, a closed-form analytical model, which includes heat loss, is needed to predict dross diameter without measuring boundary layer velocity.

Haddadi et al. [13] used empirical-based model of analysis of variance (ANOVA) to predict CO_2 LBC dross height. The input processing parameters such as laser power, cutting velocity, and existence of assisting gas were considered in a linear polynomial equation to predict polystyrene with a thickness of 0.1 mm. They reported that increasing laser power leads to a reduction of the dross height. Top and bottom kerf width was modeled with ANOVA, based on processing parameters including laser power, cutting velocity, assisting gas pressure, and thickness of polymethylmethacrylate sheet by Elsheikh et al. [14]. It was noticed that increasing thickness decreases top and bottom kerf width. Moradi et al. [15] used a numerical method to validate an experimental-based regression model for the laser cutting process of polycarbonate sheets. The effect of laser power, cutting speed, and laser focal plane, which all are energy-based processing parameters, is on the top and bottom kerf width, top heat-affected zone, and taper kerf, which were investigated by statistical techniques. Since gas-based processing parameters play a critical role in dross formation during the LBC process [16], empirical-based model is needed to cover all effective gas-based and energy-based processing parameters, which predict dross diameters.

Most of the models consider specific processing parameters such as laser power and velocity or assisting gas pressure, which is limited to a particular area. Hence, another problem is the lack of a model for LBC, which covers a global area with a meaningful definition. Moreover, austenitic stainless steel, which is one of the most valuable materials due to its corrosion resistance, should be considered in empirical-based regression LBC models. Therefore, a comprehensive study, which considers all the effective gas-based and energy-based parameters and predicts dross diameter based on these parameters, is needed.

Another objective of this paper is to develop a methodology for the integrated prediction of dross diameter of the LBC process. This methodology interprets dross diameter using a combined set of physical parameters. The approach has two main advantages; firstly, it can be used for a broad range of processing parameters without any limitation. Secondly, it provides physical insight into the LBC process, the effect of different energy-based, and gas-based processing conditions on final characteristics.

To achieve this goal, (1) energy-based processing parameters (including laser power, scanning velocity, and focal position) and (2) gas-based processing parameters (including

assisting gas pressure, workpiece distance, and the diameter of the nozzle) are considered. A set of experiments of processing parameters was conducted on thin sheet AISI 316L austenitic stainless steel to investigate variation dross diameter concerning different processing conditions of the LBC process. Dross diameters of all specimens were measured by a novel measurement setup, which their details and conditions are explained in Sect. 2. A novel analytical model, which includes heat losses, is presented based on an energy balance approach in Sect. 3.1. The presented model is validated by previous studies and experimental results. Moreover, two empirical models including, regression and combined parameters, are introduced. A regression model, which includes all effective energy-based and gas-based parameters, is verified with experimental results in Sect. 3.2. Furthermore, a set of effective physical parameters, including energy density and gas density, is introduced in Sect. 3.3. A methodology is developed to predict dross diameter based on proposed physical parameters. All models are compared with each other and experimental results in the last section to study the effectiveness of energy-based or gas-based parameters on dross diameter.

2 Experimental procedure

2.1 Experimental setup and material preparation

As shown in parts (A) and (B) of Fig. 1, the fiber laser cutting system had different parts, including gas source, optical resonator, chiller, and table. The laser beam is produced by pumping source in laser medium of the optical resonator, which is a 750 W fiber Raycus with a wavelength of 1060 nm in this work. The laser beam and assisting gas are radiated to a workpiece in a laser head. The nitrogen was used as the assisting gas to remove the melt material from the melt pool. There are collimation and focal lenses inside the head of the laser cutting machine, which the length of them is 50 mm (further explanation is provided in the Appendix). The focused spot diameter, which is the smallest diameter of laser beam coming out from the laser cutting head, is 0.15 mm.

As can be seen in part A of Fig. 1, the laser cutting process has different processing parameters, including laser power (p), scanning velocity (v), focal position (f), assisting gas pressure (g), the diameter of the nozzle (n), and workpiece distance (d). The adjustment of focal position and workpiece distance of the laser cutting machine are shown in parts D and E of Fig. 1, respectively. The workpiece distance (called nozzle stand-off distance [17] and stand-off distance [18] in previous studies) is changed by moving the laser cutting head along the z-axis with a pendant. On the other hand, adjusting the focusing lens leads to a change of the focal position (or focal plane position relative to workpiece surface [18] and focal point position [17]).

AISI 316L austenitic stainless steel sheets with a thickness of 0.8 mm and a chemical composition shown in Table 1 are used in the current experiment. All AISI 316L sheets were cut into specimen with 12 cm hexagonal shape as shown in part (C) of Fig. 1. Before, the LBC process, specimens were rinsed with water and washed with alcohol to remove any contamination.

2.2 Design of experiment

The present study aims to develop models for predicting dross formation during the LBC process based on input gas and energy. Since this property is influenced by the processing parameters, all effective gas-based and energy-based processing parameters are considered in the current research. Laser power (p), scanning velocity (v), and focal position (f) are considered energy-based processing parameters, while gas-based processing parameters of the present study are assisting gas pressure (g), the diameter of the nozzle (n), and workpiece distance (d). The variation of processing parameters is studied through 18 different specimens in the current research, which are listed in Table 2.

2.3 Dross measurement procedure

Different dross measurement methods were proposed previously, but over 71% use the fingernail test for dross measurement [19]. The fingernail test is performed using a fingernail, which is gouged at the surface. The fingernail test is not limited to a particular finger, but it is also preferred to use a thumb. According to this, it can be concluded that the mentioned methods are not applicable. Moreover, although the fingernail test is easy and fast, it is a qualitative method, which is inaccurate. Hence, the repeatability of this method is not reliable. Thus, a unified method of dross measurement, which is simple, easy to work, and accurately quantitative at the same time, is needed.

Accordingly, a dross measurement setup is presented in this study, as shown in Fig. 2. The proposed two dimensions, nondestructive and contactless process measurement method, include lamp, the BFS-120S4M camera, fixture, and system, in which details are provided in Table 3.

The camera and specimen are placed in a fixture, adjusted to provide the best focused and resolution image (see Table 4). The light is aligned to capture an image with SpinView software by a lamp. Noting, for each specimen, two front and back raw images are captured to calibrate the

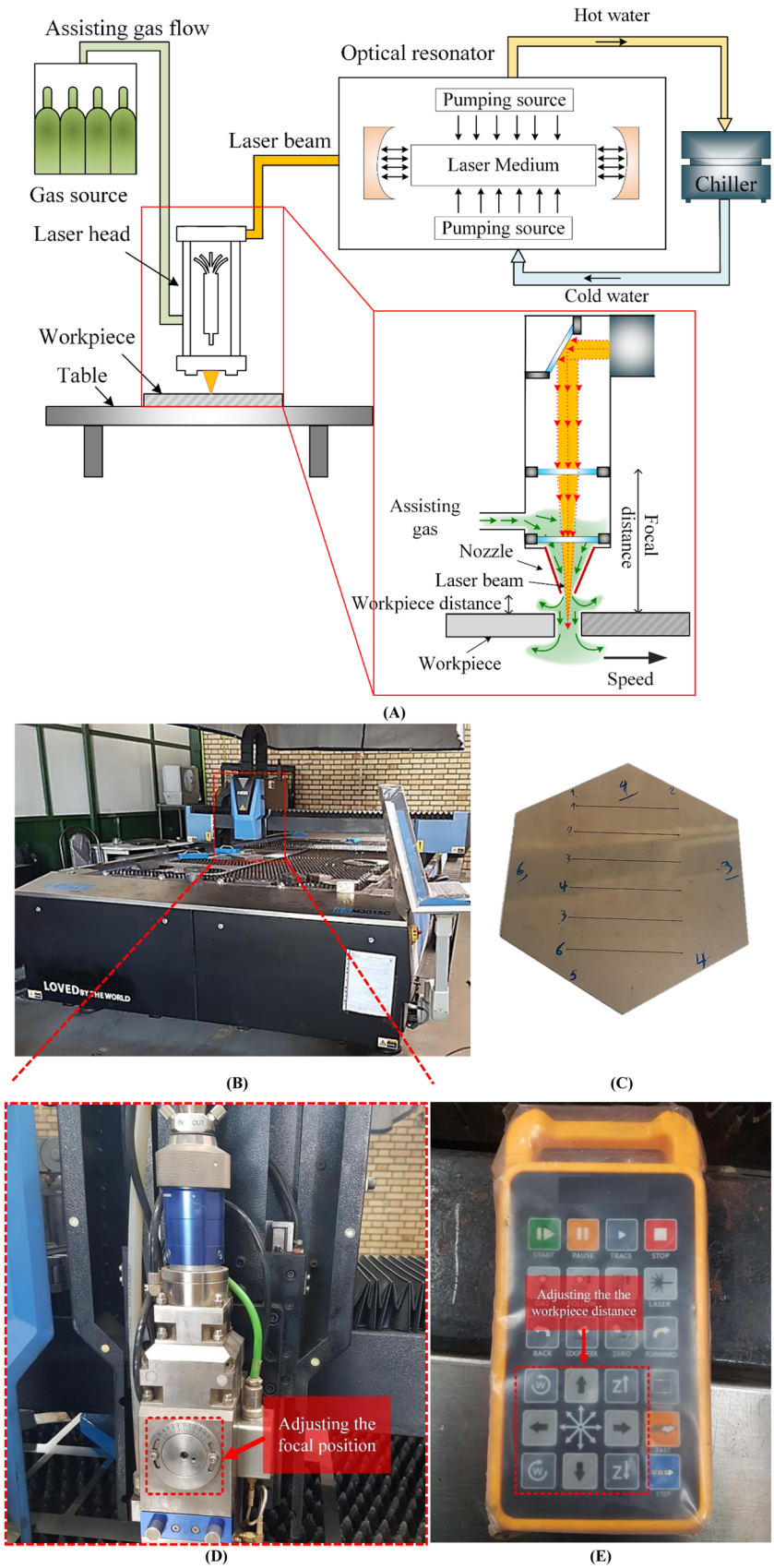

Fig. 1 The fiber laser cutting experimental set-up; **A** schematic diagram, **B** machine, **C** specimen, **D** adjustment of the focal position of the laser cutting machine, **E** adjustment of workpiece distance of laser cutting machine

Table 1 Austenitic stainless steel 316L chemical composition (wt.%)

C	Cr	Fe	Mn	Mo	Ni	P	S	Si
0.03	17.0	Balance	1.5	2.5	12.0	0.03	0.05	0.5

Table 2 The experiment specimens

Specimen	*p* (W)	*v* (m/s)	*f* (mm)	*d* (mm)	*g* (MPa)	*n* (mm)
1	600	80	2.5	0.6	0.8	1.5
2	700	80	2.5	0.6	0.8	1.5
3	750	30	2.5	0.6	0.8	1.5
4	750	40	2.5	0.6	0.8	1.5
5	750	60	2.5	0.6	0.8	1.5
6	750	130	2.5	0.6	0.8	1.5
7	750	80	0	0.6	0.8	1.5
8	750	80	5	0.6	0.8	1.5
9	750	80	2.5	0.3	0.8	1.5
10	750	80	2.5	0.6	0.8	1.5
11	750	80	2.5	1	0.8	1.5
12	750	80	2.5	1.5	0.8	1.5
13	750	80	2.5	2	0.8	1.5
14	750	80	2.5	2.5	0.8	1.5
15	750	80	2.5	0.6	0.2	1.5
16	750	80	2.5	0.6	0.5	1.5
17	750	80	2.5	0.6	0.8	1
18	750	80	2.5	0.6	0.8	2

area of dross (parts (A) and (B) of Fig. 3). The raw-captured image imports in national instrument (NI) vision assistant modulus of LabView software and then by image processing modulus, the contour of dross is extracted (part (C) of Fig. 3). The maximum dross diameters, which are observed in specimens, are provided in Table 3.

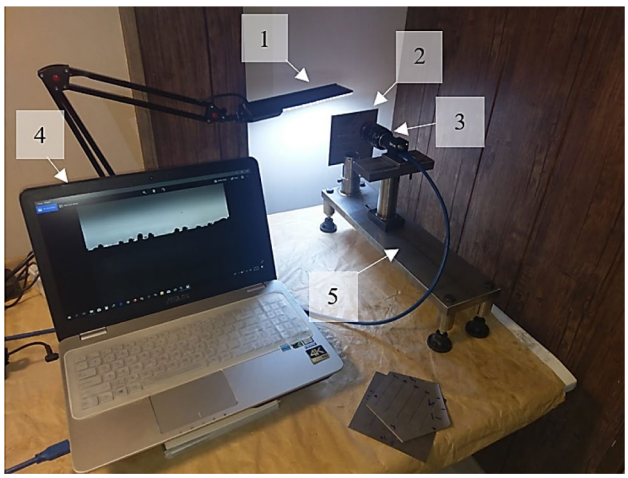

Fig. 2 Dross measurement setup

3 Results and discussion

3.1 Analytical model

The laser beam cutting (LBC) process can be classified into three stages, including heating, melting-vaporizing, and ejection, as shown in part (A) of Fig. 4. In the heating stage, the surface of the workpiece is heated up by the laser beam. The power of the laser beam leads to the formation of the molten layer and vaporizing process in the second stage. In the last stages, assisting gas is blown to the molten material and drags away in the cutting kerf [1]. Depending upon the laser beam cutting processing parameters, the molten layer thickness of the second stage varies. In addition, a jet of dross, including tiny droplets, is formed at the gas–liquid interface of the cutting kerf in the last stage of the LBC process (part B of

Table 3 The parts of dross measurement setup

Number	Name
1	Lamp
2	Specimen
3	Camera
4	System
5	Fixture

Table 4 Experimental results

Specimen	*p* (W)	*v* (m/s)	*f* (mm)	*d* (mm)	*g* (MPa)	*n* (mm)	Dross diameter(μm)
1	600	80	2.5	0.6	0.8	1.5	792.8
2	700	80	2.5	0.6	0.8	1.5	799.1
3	750	30	2.5	0.6	0.8	1.5	851.7
4	750	40	2.5	0.6	0.8	1.5	841.4
5	750	60	2.5	0.6	0.8	1.5	851.2
6	750	130	2.5	0.6	0.8	1.5	795.5
7	750	80	0	0.6	0.8	1.5	916.0
8	750	80	5	0.6	0.8	1.5	807.8
9	750	80	2.5	0.3	0.8	1.5	801.6
10	750	80	2.5	0.6	0.8	1.5	841.6
11	750	80	2.5	1	0.8	1.5	818.6
12	750	80	2.5	1.5	0.8	1.5	814.7
13	750	80	2.5	2	0.8	1.5	1062.2
14	750	80	2.5	2.5	0.8	1.5	982.7
15	750	80	2.5	0.6	0.2	1.5	856.3
16	750	80	2.5	0.6	0.5	1.5	807.2
17	750	80	2.5	0.6	0.8	1	815.5
18	750	80	2.5	0.6	0.8	2	830.9

Fig. 4) [20]. As the dross formation of the cutting kerf is associated with the molten layer thickness, an investigation into this layer during the LBC becomes essential.

The molten layer thickness involving laser beam, melting, oxidation of the assisting gas, and heat losses can be solved by numerical approaches using the differential form of conservation equation. Nevertheless, due to some unknown properties of species for metallic material, such as vapor properties, this model is difficult to use. Furthermore, a simplified closed-form model based on the equilibrium equations can be presented to predict molten layer thickness.

Regarding part (B) of Fig. 4, laser beam, melt, exothermic oxidation, and heat losses affect the molten layer thickness (S_L). The energies such as radiation, conduction, and convection are considered heat losses. To model the molten layer thickness during the laser beam cutting process, energy balance or equilibrium equation is considered as follows:

$$\dot{E}_{\text{beam}} + \dot{E}_{\text{oxidation}} = \dot{E}_{\text{melt}} + \dot{E}_{\text{cond}} + \dot{E}_{\text{conv}} + \dot{E}_{\text{rad}} \tag{1}$$

where $\dot{E}_{\text{beam}}, \dot{E}_{\text{oxidation}}, \dot{E}_{\text{melt}}, \dot{E}_{\text{cond}}, \dot{E}_{\text{conv}}$, and $\dot{E}_{\text{rad}}$ are the rate of the laser beam, exothermic oxidation reaction, melting, conduction, convection, and radiation energies, respectively. It is assumed that the produced molten layer flows in the direction of the assisting gas steadily. This flow is because of the drag force, which developed at the interface of the assisting gas melt. It is supposed that convection energy of the surface [21–25], and exothermic oxidation reaction energies are negligible compared with other energies such as laser beam, melting, conduction, and radiation energies. Since most of the energy of incident laser beam, which absorbed is spent to heat and melt of substrate [26]. It contrasts to the previous study [6], which did not consider radiation and conduction energies. The energy of melting or phase change can be provided as follows [20].

$$\dot{E}_{\text{melt}} = \dot{m}_{\text{L}}\left[C_{\text{ps}}(T_{\text{m}} - T_i) + L_{\text{m}} + \beta L_{\text{ev}} + 1.65C_{\text{pm}}(T_{\text{ev}} - T_{\text{m}})\right] \tag{2}$$

where C_{ps} and C_{pm} are the specific heat capacity of the material in the solid and melting state, respectively. The initial, molten, and evaporation temperatures of the material workpiece are shown with T_{i}, T_{m}, and T_{ev}, respectively. L_{m} and L_{ev} are the latent heating of molten and evaporation, and β is a fraction of molten metal evaporation, which evaporates from the surface at the assisting gas–melt interface [11]. Noteworthy, although by increasing laser power, the portion of evaporation materials increases, and the previous study [6] has not considered the latent heating of evaporation in melting energy of dross diameter model.

The rate of mass converted from solid into the melt at the workpiece surface is shown with $\dot{m}_{\text{L}}$, which in the LBC process, can be written as

$$\dot{m}_{\text{L}} = \frac{\partial}{\partial t}(\rho V) = \rho_{\text{L}} v_{\text{L}} A \tag{3}$$

where v_{L}, ρ_{L}, and A are the molten material velocity, the density of the molten material of the workpiece, and cross-sectional area, respectively. It is assumed that the molten

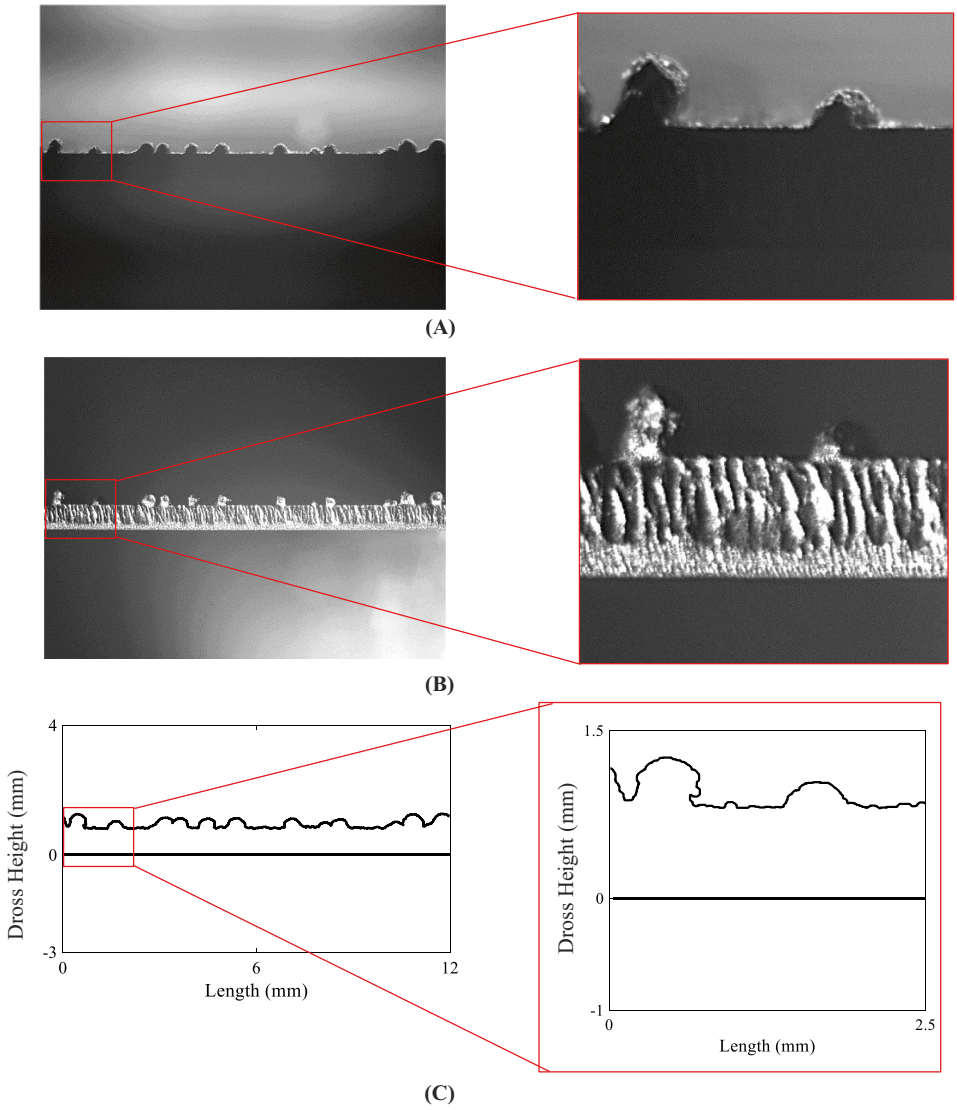

Fig. 3 The procedure of extracting data from the sample; **A** front raw image, **B** back raw image, **C** dross extracted contour

material moves towards the bottom of the workpiece. This movement is induced by shear stress (τ), which is produced by the assisting gas jet on the surface of the melt interface [12]. The velocity of melt material is given by

$$v_{\mathrm{L}} = \frac{S_{\mathrm{L}}\tau}{\mu_{\mathrm{L}}} \tag{4}$$

where S_{L} and μ_{L} are the melt layer thickness and the dynamic viscosity of the molten workpiece material, respectively. The shear stress in the LBC process is given previously as follows [12].

$$\tau = \sqrt{\frac{\rho_{\mathrm{G}}\mu_{\mathrm{G}}v_{\mathrm{G}}^3}{z}} \tag{5}$$

where ρ_{G}, μ_{G}, and v_{G} are the density, the dynamic viscosity, and the velocity of assisting gas. The thickness of the workpiece is shown with z. Substituting Eqs. (3)–(5) in Eq. (2), the melt energy is written as

$$\dot{E}_{\mathrm{melt}} = \rho_{\mathrm{L}}\left(\frac{S_{\mathrm{L}}}{\mu_{\mathrm{L}}}\sqrt{\left(\rho_{\mathrm{G}}\mu_{\mathrm{G}}v_{\mathrm{G}}^3\right)/z}\right) A\left[C_{\mathrm{P_s}}(T_{\mathrm{m}} - T_i) + L_{\mathrm{m}} + \beta L_{\mathrm{ev}} + 1.65C_{\mathrm{Pm}}(T_{\mathrm{ev}} - T_{\mathrm{m}})\right] \tag{6}$$

The rate of the laser beam, conduction, and radiation energies is considered as follows.

$$\dot{E}_{\mathrm{beam}} = p \tag{7}$$

$$\dot{E}_{\mathrm{cond}} = A_{\mathrm{Left}}h(T_{\mathrm{ev}} - T_{\mathrm{m}}) + A_{\mathrm{Right}}h(T_{\mathrm{ev}} - T_{\mathrm{m}}) = 2Ah(T_{\mathrm{ev}} - T_{\mathrm{m}}) \tag{8}$$

$$\dot{E}_{\mathrm{rad}} = 2\varepsilon\sigma\left(T_{\mathrm{ev}}^4 - T_{\mathrm{i}}^4\right) \tag{9}$$

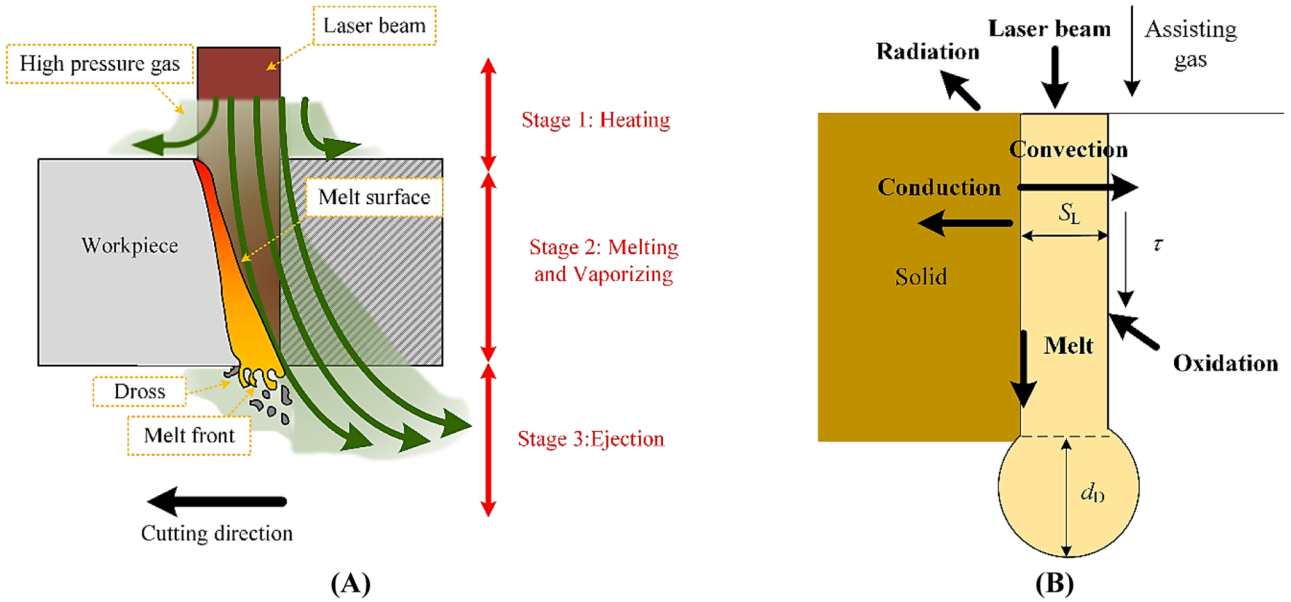

Fig. 4 Dross formation during laser beam cutting process; **A** general stages of the process, **B** schematic view of melt section

where h, ε, and σ are the thermal conductivity, the emissivity of material, and the Stefan–Boltzmann constant. Substituting Eqs. (6)–(9) into Eq. (1) gives the molten layer thickness as Eq. (10).

$$S_{\mathrm{L}}=\frac{\mu_{\mathrm{L}}\left(\frac{p}{A}-\varepsilon\sigma\left(T_{ev}^{4}-T_{i}^{4}\right)-2h(T_{m}-T_{i})\right)}{\rho_{\mathrm{L}}\left[C_{\mathrm{P_s}}(T_{\mathrm{m}}-T_{i})+L_{\mathrm{m}}+\beta L_{\mathrm{ev}}+1.65C_{\mathrm{Pm}}(T_{\mathrm{ev}}-T_{\mathrm{m}})\right]\sqrt{\rho_{\mathrm{G}}\mu_{\mathrm{G}}v_{\mathrm{G}}^{3}/z}} \tag{10}$$

can be written as a function of the molten layer thickness as follows [11].

$$d_{\mathrm{D}}=\left(\frac{3\pi}{\sqrt{2}}\right)S_{\mathrm{L}}\left(1+\frac{3\mu_{\mathrm{L}}}{\sqrt{\rho_{\mathrm{L}}S_{\mathrm{L}}}}\right)^{\frac{1}{6}} \tag{11}$$

Substituting Eq. (10) into Eq. (11), the presented analytical dross diameter model is written as

$$d_{\mathrm{D.Analytical}}=\left(\frac{3\pi}{\sqrt{2}}\right)\frac{\mu_{\mathrm{L}}\left(\frac{p}{A}-\varepsilon\sigma\left(T_{ev}^{4}-T_{i}^{4}\right)-2h(T_{m}-T_{i})\right)}{\rho_{\mathrm{L}}\left[C_{\mathrm{P_s}}(T_{\mathrm{m}}-T_{i})+L_{\mathrm{m}}+\beta L_{\mathrm{ev}}+1.65C_{\mathrm{Pm}}(T_{\mathrm{ev}}-T_{\mathrm{m}})\right]\sqrt{\rho_{\mathrm{G}}\mu_{\mathrm{G}}v_{\mathrm{G}}^{3}/z}}$$
$$\times\left(1+\frac{3\mu_{\mathrm{L}}}{\sqrt{\rho_{\mathrm{L}}\frac{\mu_{\mathrm{L}}\left(\frac{p}{A}-\varepsilon\sigma\left(T_{v}^{4}-T_{i}^{4}\right)-2h(T_{m}-T_{i})\right)}{\rho_{\mathrm{L}}\left[C_{\mathrm{P_s}}(T_{\mathrm{m}}-T_{i})+L_{\mathrm{m}}+\beta L_{\mathrm{ev}}+1.65C_{\mathrm{Pm}}(T_{\mathrm{ev}}-T_{\mathrm{m}})\right]\sqrt{\rho_{\mathrm{G}}\mu_{\mathrm{G}}v_{\mathrm{G}}^{3}/z}}}}\right)^{\frac{1}{6}} \tag{12}$$

Considering Eq. (10), it can be seen that the molten layer thickness depends on assisting gas properties, such as assisting gas velocity, density, and viscosity, as well as laser cutting properties such as power and melt material properties such as density, viscosity, and emissivity.

During the LBC process, a jet of dross is generated, consisting of metal droplets of different sizes. The droplet diameter of the molten layer, which leads to the dross diameter, was formulated earlier. Therefore, the dross diameter (d_{D})

Considering the material and assisting gas properties of Table 5, the dross diameter is analyzed and compared with the experimental and previous study results [6] for laser power in Table 6.

Considering Table 6, it can be seen that the mean of error of the presented analytical model ($d_{\mathrm{D.Analytical}}$) is less than the study [6]. The latent heating of evaporation, conduction, and radiation energies was not considered in the previous study. Although the means of error of $d_{\mathrm{D.Analytical}}$ and study

Table 5 Workpiece and assisting gas properties used in the modeling

Property	Value
The viscosity of melting material	0.9×10^{-2} N/(s.m^2)
The density of melted workpiece	7196 kg/m^3
Specific heat capacity of the material in the solid-state	330 J/(kg.K)
The melting temperature	1810 K
Latent heat of melting	2.72×10^5 J/kg
Specific heat capacity of the material in the liquid state	330 J/(kg.K)
Vaporization temperature of the material	3133
The density of assisting gas	6.875 kg/m^3 at 6 bar
The viscosity of assisting gas	61.77×10^{-6} N/(s.m^2)
The velocity of gas jet	417 m/s
Fraction of evaporation contribution	0.1
Latent heat of boiling	6.10×10^5 J/kg
The emissivity of the surface of material	0.66
Stefan–Boltzman constant	5.67×10^{-8} W/(m^{2}K^4)
Thermal conductivity of material	27 W/(m.K)
Initial temperature	298.15 K

Table 6 The experimental, presented analytical model and previous study results of dross diameter (μm)

Power				
	600	**700**	**750**	**Mean of error (%)**
Method				
$d_{\text{D. Study}}$ [6]	736.73	859.22	920.46	8.00
$d_{\text{D. Analytical}}$	718.46	837.92	897.64	6.96
Experimental	792.80	799.10	841.60	-

[6] are near, the manner of them for power is different, as shown in Fig. 5.

According to Fig. 5, the error of the presented analytical model decreases with a slope of − 0.02 by increasing the laser power. It is in contrast to the previous study [6], in which an increase in laser power leads to increasing of error with the slope of + 0.01. As the laser power increases, the temperature of molten material increases [27]. Furthermore, the emissivity of surface and thermal conductivity of material increase by an increase of temperature [28, 29]. Thus, the portion of laser beam energy converts to radiation and conduction energies increases, and the error of the

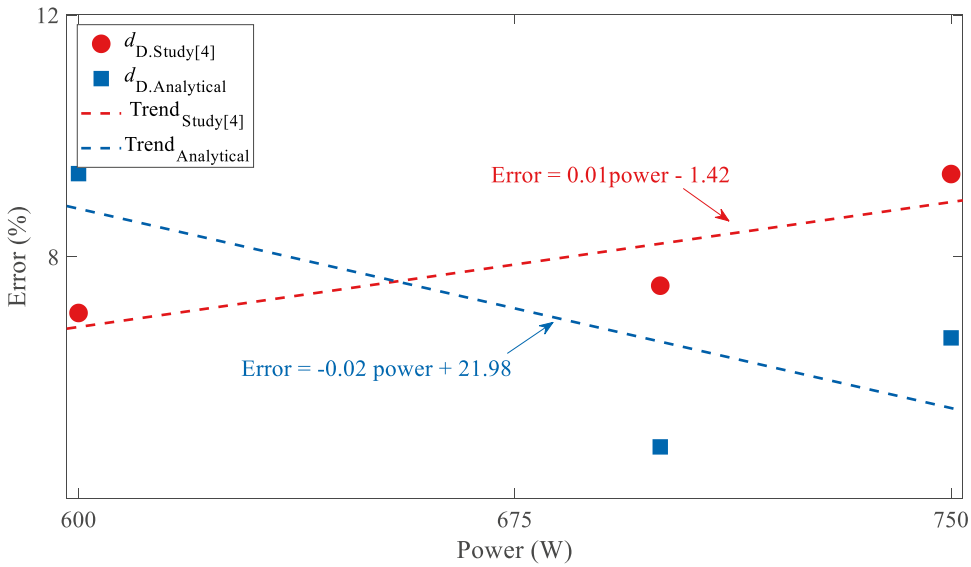

Fig. 5 Dross diameter error of presented analytical model and study [6] versus laser power in LBC process

Table 7 The experimental, presented regression model results of dross diameter (μm)

Test specimens	Experimental	$d_{\mathrm{D.Reg}}$	Error (%)
10	841.60	821.80	0.02
5	851.20	832.70	0.02

presented analytical model decreases. Noting, since the error of the presented analytical model decreases with the slope of two times larger than a slope of the study [6], the presented model is more accurate for the high-power LBC process.

3.2 Empirical models

3.2.1 Regression model

Regression modeling is one of the fundamental statistical methods that predict output within the range of input values in the dataset for model-fitting or interpolation. The multiple linear regression model, which has been used in the present study, gives insight into relationships between processing parameters of the laser cutting process [30]. In this model, the regression coefficients are provided to meet the law of dimensional consistency [30]. This law of dimensional consistency of regression model has been investigated for kerf width [14, 15, 27], heat-affected zone (HAZ) [15, 27, 31], kerf taper angle [14, 15, 27], and surface roughness [32, 33] of laser cutting process in previous studies. Despite previous study [13], all energy-based processing parameters, including laser power (p), scanning velocity (v), and focal position (f), and gas-based processing parameters including workpiece distance (d), the diameter of the nozzle (n), and gas amplitude (g) are considered to construct regression model. This model is valuable to compare which gas-based and energy-based processing parameters affect the dross diameter of the LBC process more. The presented regression dross diameter ($d_{\mathrm{D.Reg}}$) is as follows.

$$d_{\mathrm{D.Reg.}} = \overline{\beta}_0 + \overline{\beta}_1 p + \overline{\beta}_2 v + \overline{\beta}_3 f + \overline{\beta}_4 d + \overline{\beta}_5 g + \overline{\beta}_6 n \tag{13}$$

$$\begin{cases} \overline{\beta}_0 = 0.833\,[\mu\mathrm{m}] \\ \overline{\beta}_1 = 0.000046\,[\frac{\mu\mathrm{m}}{\mathrm{W}}] \\ \overline{\beta}_2 = -0.000545\,[\frac{\mu\mathrm{m}}{\mathrm{m/s}}] \\ \overline{\beta}_3 = -0.0216\,[\frac{\mu\mathrm{m}}{\mathrm{mm}}] \\ \overline{\beta}_4 = 0.0967\,[\frac{\mu\mathrm{m}}{\mathrm{mm}}] \\ \overline{\beta}_5 = -0.0365\,[\frac{\mu\mathrm{m}}{\mathrm{MPa}}] \\ \overline{\beta}_6 = 0.0154\,[\frac{\mu\mathrm{m}}{\mathrm{mm}}] \end{cases} \tag{14}$$

The presented regression model ($d_{\mathrm{D.Reg.}}$) is based on 16 trained specimens shown in Table 3. Two random specimens were considered to verify, as provided in Table 7. Comparing the results of $d_{\mathrm{D.Reg.}}$ with experimental results, the corresponding error is about 0.02 for both test specimens. Thus, it is concluded that the presented regression model follows experimental results with good accuracy.

The analysis of variance (ANOVA) table, including the degree of freedom (DF), the sum of squares (SS), and means squares (MS), is demonstrated in part (A) of Fig. 6. The ANOVA table shows that the effect of processing parameters is different. By dividing processing parameters into gas-based processing parameters including workpiece distance (d), the diameter of the nozzle (n), and assisting

Source	DF	SS (×0.01)	MS (×0.01)
p	1	0.01	0.02
v	1	0.19	0.19
f	1	0.58	0.58
d	1	4.84	4.84
g	1	0.05	0.05
n	1	0.01	0.01
Total	6	5.89	0.98

(A)

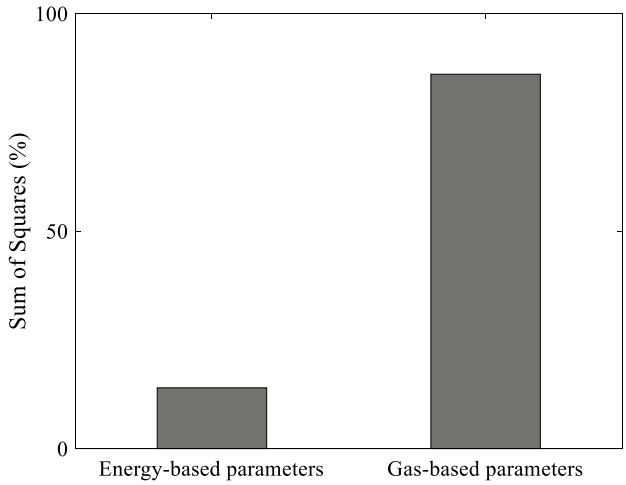

(B)

Fig. 6 **A** Analysis of variance (ANOVA) of dross diameter, **B** sum of squares of dross diameter for energy-based and gas-based parameters

gas pressure (g), and energy-based processing parameters including laser power (p), scanning velocity (v), and focal position (f), a valuable result can be investigated. As shown in part (B) of Fig. 6, the sum of the square of gas-based processing parameters (86%) is more significant than the energy-based processing parameters, which is 14%. Therefore, it can be concluded that gas processing parameters play a more critical role than energy-based processing parameters in the formation of dross during the LBC process. Previous analytical studies also revealed that dross formation is dominated by assisting gas processing parameters [6, 20].

3.2.2 Physical parameter model

The change of processing parameters leads to a variation in dross diameter as seen in previous sections. Processing parameters possess two main challenges. Firstly, they are restricted to a narrow and local range in which experiments are conducted. Secondly, they do not provide physical insight into the process. Therefore, a more general modeling approach is required to provide an in-depth physical meaning of the process. Models based on physical rather than processing parameters can overcome shortcomings mentioned above. In this section, the dross diameter of the LBC process will be analyzed based on physical parameters and the described combined parameter, in order to gain a detailed insight into the process.

Effective physical parameters To construct the physical-based model, the first step is to determine effective physical parameters regarding energy-based and gas-based processing parameters. Since, few studies have been focused on these parameters, two novel physical parameters, including the energy density (ED) and gas density (GD), are introduced for the LBC process. The energy and gas density formulations are provided as follows:

$$ED = \frac{4p}{\pi va} \left[\mathrm{J/mm^2}\right] \tag{15}$$

$$GD = \frac{4g}{\pi dn} \left[Pa/\mathrm{mm^2}\right] \tag{16}$$

p, v, and a define the laser power, velocity, and beam diameter, respectively. The assisting gas pressure, the diameter of the nozzle, and the workpiece distance are shown by g, n, and d, respectively. The energy density (ED), which combines energy-based processing parameters, defines the amount of energy deposited per unit area during the LBC process. Considering $\pi/4$ in the denominator of gas density formula is because of formulation of a circular area of the beam diameter. On the other hand, the density of the gas, which radiates on a specific area, is interpreted by gas density (GD). Considering $\pi/4$ in the denominator of energy density formula is because of formulation of a circular area of nozzle diameter. Similarly, gas density combines gas-based processing parameters of the LBC process.

These physical parameters take into account the effect of three input processing parameters simultaneously in two different terms of energy and gas, which affects dross during the LBC process. In other words, the processing parameters are separated into two energy and gas physical parameters.

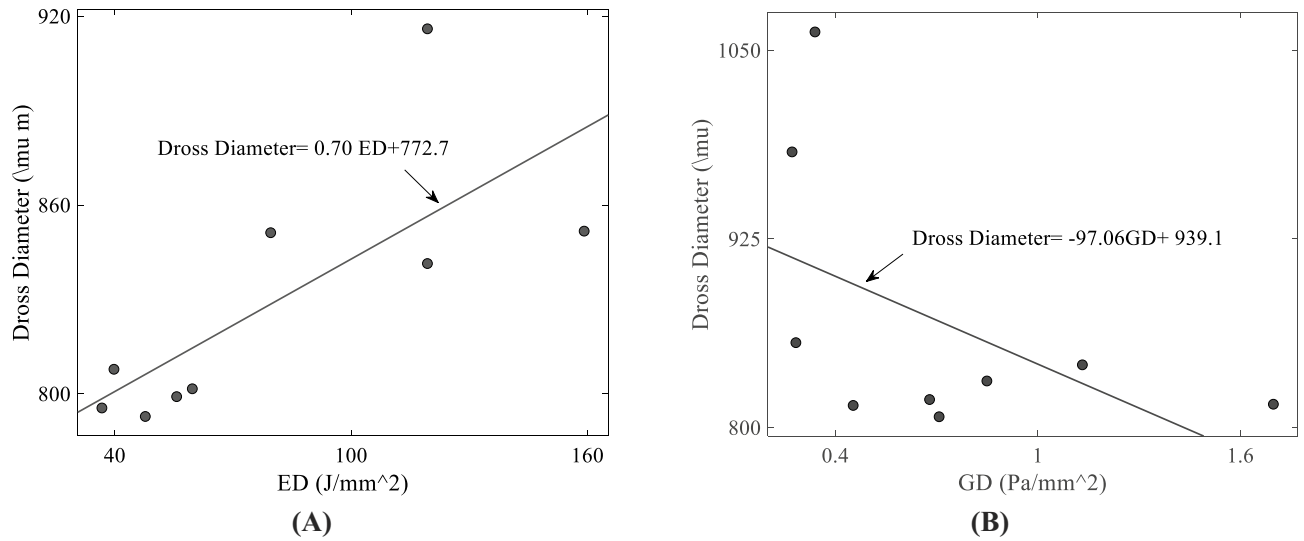

Fig. 7 The effect of physical parameters on dross diameter in LBC process. **A** Dross diameter versus energy density with constant $GD = 1.13$ Pa/mm^2, **B** dross diameter versus gas density with constant $ED = 59.68$ J/mm^2

Table 8 The experimental and presented combined parameter model constants and results

CP constants	m	n	p_1 [$mm^{2(m+n)+1}/Pa^m.J^n$]	p_2 [mm]
Value	−1.09	1.03	0.67	769.80
Test specimens	**Experimental**	$d_{D.CP}$	**Error (%)**	
5	851.20	823.23	3.28	
10	841.60	809.53	3.81	

Here, to investigate the effectiveness of the presented physical parameters, the experimentally measured dross diameter as a function of corresponding energy and gas densities is shown in parts (A) and (B) of Fig. 7.

Different results can be concluded from Fig. 7. Firstly, since the slopes of the trend of energy and gas densities graph on dross diameter are non-zero, they affect it directly in the LBC process. Secondly, since the slope of gas density is 138.66 times larger than the slope of energy density, it is more effective than energy density. This result agrees with the results of regression and analytical models, which are presented in previous sections. Thirdly, as the signs of the slope of physical parameters trends are different, it can be concluded that to provide a small dross diameter, it is needed to decrease energy density (because of the slope of + 0.7) and increase gas densities (because of the slope of − 97.06). Considering the provided results, it can be concluded that the presented physical parameters are selected correctly, and a model can be constructed based on them in the next section.

Combined physical parameter model While physical parameters such as the energy and gas densities are required to understand the characteristics of the LBC process, it is beneficial to combine these parameters into a single compact form to develop a more general and straightforward framework. Such a compact form can be defined as a new combined parameter. In the current methodology, a unique combined parameter (CP) is considered in the following form:

$$CP = GD^m ED^n \tag{17}$$

in which GD and ED define the gas and energy densities, and m and n define the degree of importance for each of these physical parameters, respectively. Under the current methodology, the constant values m and n are calculated based on a correlation between the CP value and experimental dross diameter. In other words, it is defined as a function of the combined parameter as follows:

$$d_{D.CP} = p_1 \times CP + p_2 + \text{Error} \tag{18}$$

$$\begin{cases} p_1 = \left[\left(\frac{mm^2}{Pa}\right)^m \left(\frac{mm^2}{J}\right)^n mm\right] = \left[\frac{mm^{2(m+n)+1}}{Pa^m J^n}\right] \\ p_2 = [\text{mm}] \end{cases} \tag{19}$$

where p_1 and p_2 are constants of a combined parameter model ($d_{D.CP}$). These coefficients are provided based on regression analysis to meet the law of dimensional consistency. Using general optimization techniques, optimized m and n values are calculated to minimize the error or maximize R-squared (R^2) value. The maximum R-squared is provided when $m = -1.09$ and $n = 1.03$ in Eq. (17). A more detailed explanation of $d_{D.CP}$ is provided in Table 8. The dross diameter of the LBC process is analyzed based on

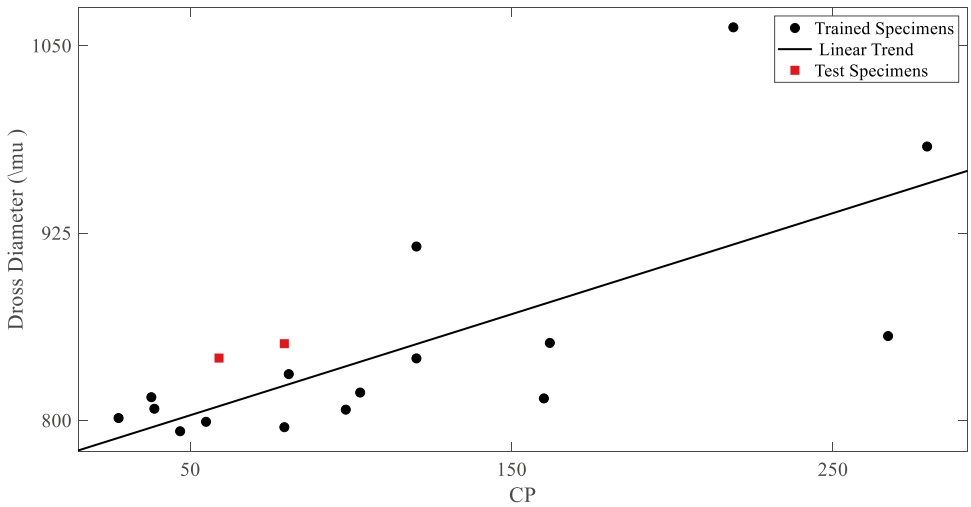

Fig. 8 Dross diameter versus combined parameter model in LBC process

the optimized combined parameters with trained specimens, which is shown in Fig. 8. Two random test specimens are considered (shown with the red square shape) to compare the $d_{D.CP}$ with experimental results, which are presented in Table 8.

According to Table 8, the error of the combined parameter model is less than 4% in both test specimens. This approves the accuracy and validation of the presented combined parameter model. Since m is negative and n is positive, it can be concluded that an increase in gas density and decrease of energy densities lead to a decrease of dross diameter in the LBC process. Similarly, as m is more considerable than n, it can be deducted that gas density affects dross diameter more than energy density. These findings agree with Fig. 7, which approves the correctness of the presented combined parameter model.

3.3 Comparison of models

3.3.1 Parameter study

Considering previous sections, the analytical and two empirical regression and combined parameter models were introduced to predict dross diameter in the laser beam cutting process. To investigate further, the results of presented models for experimental results versus laser scanning velocity and power are shown in parts (A) and (B) of Fig. 9, respectively.

Considering Fig. 9, different results can be concluded. Firstly, by increasing laser scanning velocity, the dross diameter reduces in all three experimental, combined parameter, and regression models results (part (A) of Fig. 9). This is in agreement with a previous study [6]. Lower cutting velocity results in higher molten materials because the incident laser beam lasts longer in the same area. In the laser cutting process, the assisting gas removes away molten materials. The lower the cutting velocity, the more time (or higher velocity gas) is needed in assisting gas ejecting the melt material, which increases the dross diameter. It should be noted that since the variation of scanning velocity affects dross diameter indirectly in the analytical model (Eq. (12)), it is not considered in part (A) of Fig. 9.

Secondly, considering part (B) of Fig. 9, it can be seen that the higher laser power results in a larger dross diameter in all presented models and experimental results. This is in line with results showed by previous studies [6, 13, 20] since the increase of power leads to an increase of the molten layer thickness that enhances the higher dross diameter. Therefore, increasing laser power and decreasing scanning velocity lead to an increase in dross diameter in the LBC process. Thirdly, the presented models follow the experimental results with different accuracy.

3.3.2 The error studies

To compare models, the error of them versus laser scanning velocity and power is provided in Fig. 10.

According to part (A) of Fig. 10, it can be seen that errors of combined parameter and regression models are increased with the slope of 0.09 and 0.05 by increasing scanning velocity, respectively. It indicates that both the presented models are appropriate for low laser scanning velocity. Noting, for the same rate of decrease of laser scanning velocity, the result of the combined parameter model decreases 1.80 times smaller than the regression model. Therefore, the error of the combined parameter model leads to zero faster than the regression model during the LBC process.

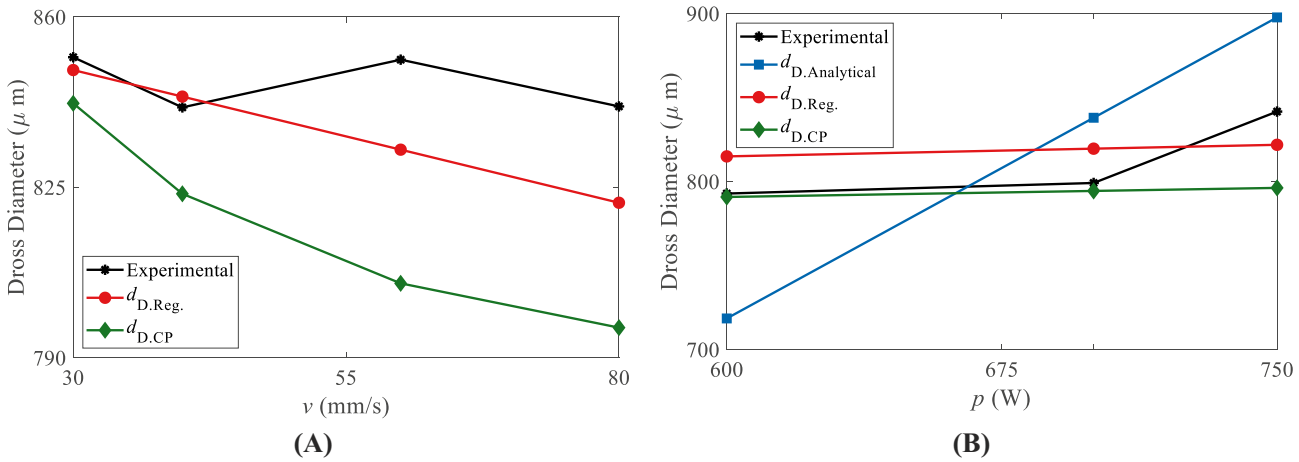

Fig. 9 Experimental results, regression, combined parameter, analytical models versus; **A** laser scanning velocity while other processing parameters are constant, **B** laser power of dross diameter while other processing parameters are constant in laser beam cutting process

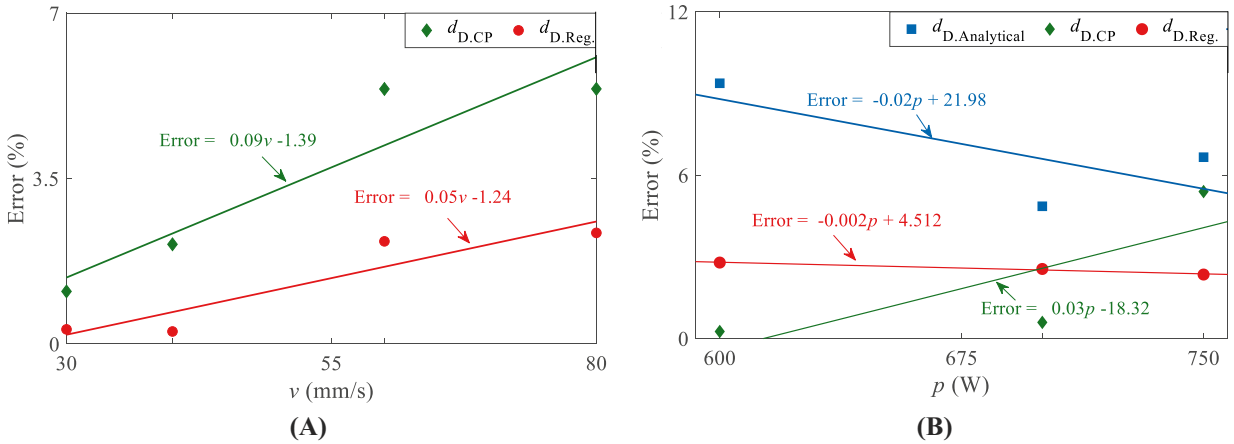

Fig. 10 The error of the regression, combined parameter and analytical models versus; **A** laser scanning velocity while other processing parameters are constant, **B** laser power while other processing parameters are constant

Considering part B of Fig. 10, some results can be investigated. Firstly, since the error's trend of regression and analytical models decrease by increasing laser power, these models are appropriate for high-power conditions (700 W < power). Noting, as the slope of error trend of the analytical model is ten times larger than the regression model, the error of the analytical model decreases faster than the regression model. Thus, for a broadband region of the high-power LBC process, the analytical model leads to small dross diameter faster. Secondly, the combined parameter model has good accuracy and error of less than 3% for low-power conditions (700 W > power). Thus, it is recommended to use a combined parameter model for low-power LBC process.

Besides energy-based and gas-based processing parameters, there are laser beam–based processing parameters, including laser wavelength [34], angle of incidence [34], sheet thickness [34], and the polarization mode of the laser beam [35]. These processing parameters affect the laser beam absorptivity of laser cutting process. The presented models can be performed to analyze the effect of laser beam–based processing parameters on dross formation or other cut properties in the future studies. Furthermore, a general optimization technique was carried out to optimize the coefficient of models since it was not the aim of the present study and other optimization techniques, including Fuzzy logic [36] and artificial neural networks [37].

4 Summary

Dross diameter during the laser beam cutting (LBC) of a metallic workpiece is considered. The processing parameters, which affect dross diameter, were divided into energy-based and gas-based categories. Two types of novel analytical-based and empiricial-based methods, including analytical, regression, and combined parameter models, were constructed based on energy and gas-based processing parameters. The analytical model was developed based on an energy balance approach, which includes conduction, radiation, and evaporation energy losses in addition to the laser beam and melting energies. A regression model was considered to study the significance of energy-based and gas-based processing parameters on the laser beam cutting process. A set of novel physical parameters, including the energy and gas densities, was proposed to provide a physical insight into the process. A set of laser cutting experiments was conducted on an austenitic stainless steel 316L workpiece sheet to validate the proposed models. The following interesting results were concluded from the developed models:

- The introduced regression model has an error of less than 4%. Furthermore, it is clear from the finding that the accuracy of the regression model increases with an increase of laser power and decrease of scanning velocity.
- The proposed analytical model is more accurate than the previous study. Since the increase of laser power leads to reduction of developed model, it can be concluded that the heat loss increases with increase of laser power.
- The presented physical parameter model could predict the dross diameter of the LBC process with the error of less than 6%. Moreover, the error of it decreases with a decrease in laser power and scanning velocity.

Experimental and all three modeling results reveal that the dross diameter is dominated by gas-based processing parameters such as assisting gas pressure and workpiece distance rather than energy-based parameters. This surprising result is clearly approved with the regression model in which gas-based processing parameters affect 86% of dross diameter during the LBC process.

Appendix

The collimation and focal lenses are two lenses, which are inside of laser cutting head. The collimation length, which is shown with d_1 in Fig. 11, affects the divergence of the beam incident on the focusing lens. The focal length (shown with d_3 in Fig. 11) also affects the geometrical parameters of the location of focused spot diameter [38]. The focused spot diameter is the smallest diameter of laser beam, which come out from the laser cutting head. In the present study, the collimation length and the focal length of laser cutting head were both 50 mm. The focused spot diameter of laser beam also is 0.15 mm.

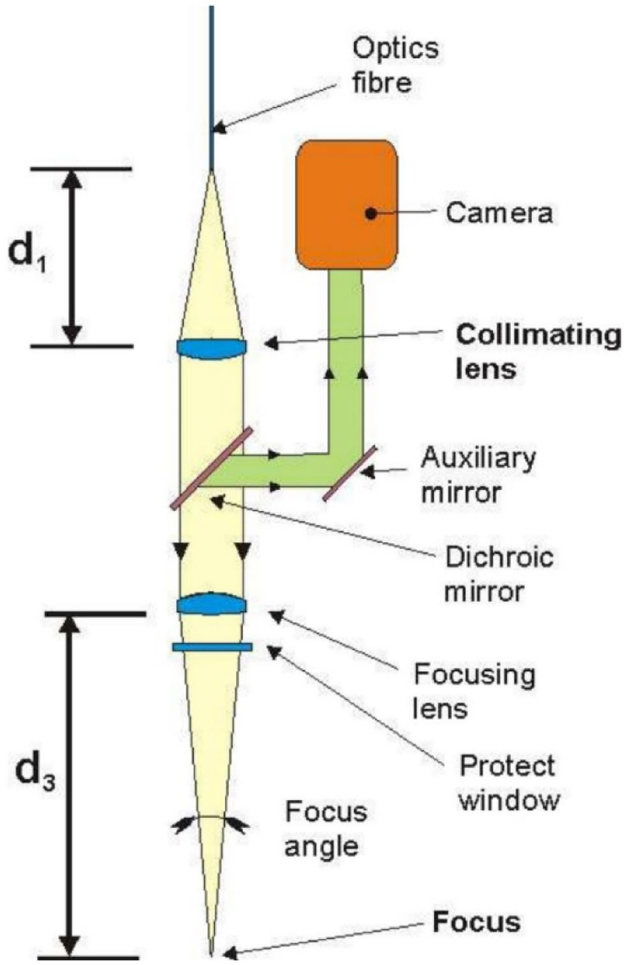

Fig. 11 The collimation length (d_1) and focal length (d_2) of laser cutting head [38]

Author contribution All authors contributed to the study's conception and design. Material preparation, data collection, and analysis were performed by Seyedeh Fatemeh Nabavi, Mohammad Hossein Farshidianfar, Anooshiravan Farshidianfar, and Saeed Marandi. The first draft of the manuscript was written by Seyedeh Fatemeh Nabavi, and all authors commented on previous versions of the manuscript. All authors read and approved the final manuscript.

Funding This study is provided under fund support of Taha Ghaleb Toos (TGT) Co. through grant number of 2020.04.07.LSR01.

Availability of data and material Not applicable.

Code availability Not applicable.

Declarations

Ethics approval Not applicable.

Consent to participate Not applicable.

Consent for publication Not applicable.

Conflict of interest The authors declare no competing interests.

References

1. Steen WM, Mazumder J (2010) Laser material processing. springer science & business media
2. Ghavidel AK, Zadshakouyan M (2017) Dimensional accuracy of CNTs/PMMA parts and holes produced by laser cutting. International Journal of Mechanical and Industrial Engineering 11(10):1736–1741
3. Karimzad Ghavidel A, Shabgard M, Biglari H (2016) Microscopic and mechanical properties of semi-crystalline and amorphous polymeric parts produced by laser cutting. J Appl Polym Sci 133(44)
4. Mushtaq RT, Wang Y, Rehman M, Khan AM, Mia M (2020) State-of-the-art and trends in CO2 laser cutting of polymeric materials—a review. Materials 13(17):3839
5. Sharma A, Yadava V (2018) Experimental analysis of Nd-YAG laser cutting of sheet materials–a review. Opt Laser Technol 98:264–280
6. Teixidor D, Ciurana J, Rodriguez CA (2014) Dross formation and process parameters analysis of fibre laser cutting of stainless steel thin sheets. The International Journal of Advanced Manufacturing Technology 71(9–12):1611–1621
7. Ko S-L, Dornfeld DA (1991) A study on burr formation mechanism. J Eng Mater Technol 113(1):75–87
8. Gillespie LK, Blotter P (1976) The formation and properties of machining burrs. Journal of Engineering for Industry 98(1):66–74
9. Wee LM, Li L (2005) An analytical model for striation formation in laser cutting. Appl Surf Sci 247(1–4):277–284
10. Ko S-L, Chang J-E, Yang G-E (2003) Burr minimizing scheme in drilling. J Mater Process Technol 140(1–3):237–242
11. Yilbas B, Aleem BA (2006) Dross formation during laser cutting process. J Phys D Appl Phys 39(7):1451
12. Schuöcker D, Aichinger J, Majer R (2012) Dynamic phenomena in laser cutting and process performance. Phys Procedia 39:179–185
13. Haddadi E, Moradi M, Ghavidel AK, Ghavidel AK, Meiabadi S (2019) Experimental and parametric evaluation of cut quality characteristics in CO2 laser cutting of polystyrene. Optik 184:103–114
14. Elsheikh AH, Deng W, Showaib EA (2020) Improving laser cutting quality of polymethylmethacrylate sheet: experimental investigation and optimization. J Market Res 9(2):1325–1339
15. Moradi M et al (2021) Simulation, statistical modeling, and optimization of CO2 laser cutting process of polycarbonate sheets. Optik 225:164932

16. Riveiro A et al (2019) Laser cutting: a review on the influence of assist gas. Materials 12(1):157
17. Wandera C, Kujanpaa V (2010) Characterization of the melt removal rate in laser cutting of thick-section stainless steel. J Laser Appl 22(2):62–70
18. Sobih M, Crouse P, Li L (2007) Elimination of striation in laser cutting of mild steel. J Phys D Appl Phys 40(22):6908
19. Franke V, Leitz L, Aurich J (2010) "Burr measurement: a round robin test comparing different methods", in *Burrs-Analysis*. Springer, Control and Removal, pp 167–178
20. Yilbas BS, Aleem BA (2006) Dross formation during laser cutting process. J Phys D Appl Phys 39(7):1451
21. Quintero F, Varas F, Pou J, Lusquiños F, Boutinguiza M, Soto R, Pérez-Amor M (2005) Theoretical analysis of material removal mechanisms in pulsed laser fusion cutting of ceramics. J Phys D Appl Phys 38(4):655
22. Modest M, Abakians H (1986) Evaporative cutting of a semi-infinite body with a moving CW laser. J Heat Transfer 108(3):602–607
23. Teixidor D, Ciurana J, Rodriguez CA (2014) Dross formation and process parameters analysis of fibre laser cutting of stainless steel thin sheets. Int J Adv Manuf Technol 71(9–12):1611–1621
24. Hsu MJ, Molian PA (1994) Thermochemical modelling in CO 2 laser cutting of carbon steel. J Mater Sci 9(21):5607–5611
25. Luo Y et al (2016) Modeling of vapor-to-melt ratio in laser cutting aluminum alloy sheet. Mach Sci Technol 20(1):44–61
26. Li Y, Latham WP, Kar A (2001) Lumped parameter model for multimode laser cutting. Opt Lasers Eng 35(6):371–386
27. Sharifi M, Akbari M (2019) Experimental investigation of the effect of process parameters on cutting region temperature and cutting edge quality in laser cutting of AL6061T6 alloy. Optik 184:457–463
28. Bergman TL, Incropera FP, DeWitt DP, Lavine AS (2011) Fundamentals of heat and mass transfer. John Wiley & Sons
29. Pichler P, Simonds BJ, Sowards JW, Pottlacher G (2020) Measurements of thermophysical properties of solid and liquid NIST SRM 316L stainless steel. J Mater Sci 55(9):4081–4093
30. Montgomery DC, Runger GC (2018) Applied statistics and probability for engineers. Wiley Hoboken, NJ
31. Parthiban A, Dhanasekaran C, Sivaganesan S, Sathish S (2020) Modeling on surface cut quality of CO2 laser cutting for austenitic stainless steel sheet. Materials Today: Proceedings 21:823–827
32. Gautam P, Singh KJMTP (2018) Experimental investigation and modeling of heat affected zone and surface roughness in erbium-doped fiber laser cutting of CFRP composite. Materials Today: Proceedings 5(11):24466–24475
33. Sharma A, Yadava V (2012) Modelling and optimization of cut quality during pulsed Nd: YAG laser cutting of thin Al-alloy sheet for straight profile. Opt Laser Technol 44(1):159–168
34. Mahrle A, Lütke M, Beyer E (2010) Part C: Journal of Mechanical engineering science. Fibre laser cutting: beam absorption characteristics and gas-free remote cutting. Proc Inst Mech Eng C J Mech Eng Sci 224(5):1007–1018
35. Niziev VG, Nesterov AV (1999) Influence of beam polarization on laser cutting efficiency. J Phys D Appl Phys 32(13):1455
36. Pandey AK, Dubey AK (2011) Intelligent modeling of laser cutting of thin sheet. International Journal of Modeling and Optimization 1(2):107
37. Madić M, Radovanović M (2013) Application of RCGA-ANN approach for modeling kerf width and surface roughness in CO 2 laser cutting of mild steel. J Braz Soc Mech Sci Eng 35(2):103–110
38. Mrňa L, Šarbort M, Řeřucha Š, Jedlička P (2013) Adaptive optics for control of the laser welding process. in EPJ Web of Conferences, vol. 48, p. 00017: EDP Sciences